Tailorable Zero-Phase Delay of Subwavelength Particles toward Miniaturized Wave Manipulation Devices

Qian Zhao, Zongqi Xiao, Fuli Zhang, Junming Ma, Ming Qiao, Yonggang Meng, Chuwen Lan, Bo Li, Ji Zhou, Peng Zhang, Nian-Hai Shen, Thomas Koschny, and Costas M. Soukoulis*

Precise and tunable manipulation of light propagation, though difficult to realize by conventional optical elements based on the uniform medium, has long been pursued.[1–4] As a major breakthrough in controlling the propagation of electromagnetic (EM) waves, metamaterials have overcome the limitations of natural materials by manipulating their chemical composition and physical properties in order to exhibit extraordinary EM phenomena, such as negative refraction,[5–9] near-zero-refraction,[10–12] subwavelength-focusing,[13–15] invisible cloaking,[16–18] and metasurfaces.[19] However, to date, these subwavelength scatterers rely mostly on anisotropic metallic patterns. An alternative approach is to use high-permittivity dielectric particles based on Mie resonances as isotropic subwavelength unit cells, which are easy to fabricate, free of Ohmic loss, and polarization independent for a broad range of angles.[20–22] Significant progress has been achieved using these subwavelength dielectric particles for wave manipulation.[23–29] In order to obtain these properties, the magnetic dipole responses of dielectric particles from microwave to visible frequencies were experimentally investigated.[23–26] The discovered resonances have been applied in order to observe controllable scattering effects from a single particle, such as the zero-backward and almost zero-forward scatterings.[27–29]

Prof. Q. Zhao, Z. Xiao, J. Ma, M. Qiao, Prof. Y. Meng
State Key Laboratory of Tribology
Department of Mechanical Engineering
Tsinghua University
Beijing 100084, China
E-mail: zhaoqian@mail.tsinghua.edu.cn

Prof. F. Zhang
Key Laboratory of Space Applied Physics and Chemistry
Ministry of Education and Department of Applied Physics
School of Science
Northwestern Polytechnical University
Xi'an 710072, China

C. Lan, Prof. B. Li, Prof. J. Zhou
State Key Laboratory of New Ceramics and Fine Processing
School of Materials Science and Engineering
Tsinghua University
Beijing 100084, China

P. Zhang, Dr. N.-H. Shen, Prof. T. Koschny, Prof. C. M. Soukoulis
Ames Laboratory and Department of Physics and Astronomy
Iowa State University
Ames, IA 50011, USA

Prof. C. M. Soukoulis
Institute of Electronic Structure and Lasers (IESL)
FORTH
71110 Heraklion, Crete, Greece

DOI: 10.1002/adma.201502298

With the increasing requirements of device miniaturization and the need for on-chip optical components, single-particle or single-layer subwavelength devices are highly sought after, especially those which can avoid complicated mechanisms such as diffraction in bulk structural media. However, most existing research on particle-based light control has focused on the utilization of single particle[28,29] or multiparticle nanoantenna.[30] In these cases, the ratio of the modulated wavelength (λ) to the particles size (l) is about 4, i.e., $\lambda/l \approx 4$, thus hindering device miniaturization. One method of realizing smaller components is to weaken the coherence effect between the magnetic and electric dipoles by increasing the ratio of wavelength to the particle size (**Figure 1**). The long-wavelength approximation can be satisfied and novel phenomenon such as an isotropic near-zero index, achieved through near-zero permeability (MNZ), can be observed. These near-zero index materials possess many interesting wave manipulation features and have been demonstrated using different mechanisms[31–35] such as epsilon-near-zero materials based on metallic structures,[32,33] Dirac cones in photonic crystals,[34] and hyperbolic materials.[35] Importantly, the media employed to achieve these phenomena are not necessarily preferred, as photonic crystals have dimensions on the same order of the targeted wavelength and hyperbolic materials exhibit an anisotropic zero-index, inside which the wave vibrates with the phase, just like in the air. So far, near-zero isotropic media resulting from an MNZ has yet to be realized. In addition, equiphase propagation for a cylindrical source in a sample, especially for a subwavelength-layered structure, has not been experimentally demonstrated. Furthermore, these Mie resonant, dielectric particles possess tunability under external stimuli that can lead to the possibility of interesting adjustable wave-control devices.[36] In this work, an isotropic zero-index medium with subwavelength dimensions and no phase delay will be studied for its potential applications in the miniaturization of wave-manipulating components.

Light scattering by small (relative to the incident light wavelength) spherical particles is a fundamental topic in classical electrodynamics and is based upon the exact Mie solution of the diffraction problem.[37] The scattered field of a single isolated dielectric sphere with radius r_0 and refractive index n can be decomposed into a multipole series with the 2^m-pole term of the scattered electric field proportional to

$$a_m = \frac{n\psi_m(nx)\psi'_m(x) - \psi_m(x)\psi'_m(nx)}{n\psi_m(nx)\xi'_m(x) - \xi_m(x)\psi'_m(nx)} \quad (1)$$

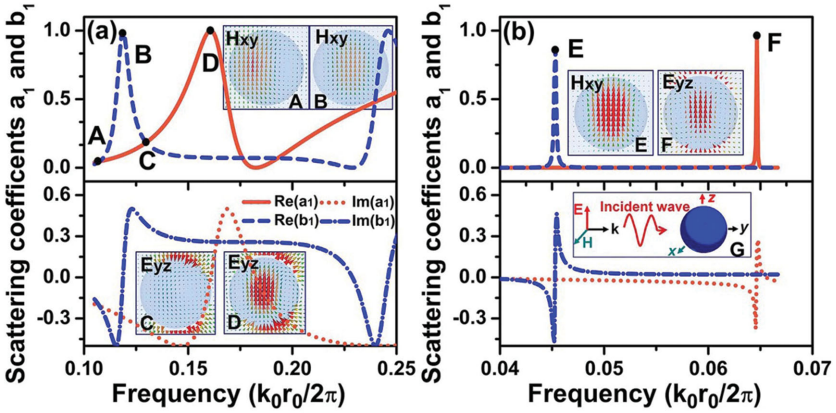

Figure 1. Scattering coefficients a_1 and b_1 with different size and permittivity of spherical particles. a) Coherent: $r_0 = 9.00$ mm, $\varepsilon = 16.5$; b) Noncoherent: $r_0 = 1.00$ mm, $\varepsilon = 120+0.1i$. Insets (A–F) show the electric or magnetic fields corresponding to points (A–F) in the frequency spectra, and inset (G) shows the schematic of interaction between dielectric particle and incident wave.

whereas the 2^m-pole term of the scattered magnetic field is proportional to

$$b_m = \frac{\psi_m(nx)\psi'_m(x) - n\psi_m(x)\psi'_m(nx)}{\psi_m(nx)\xi'_m(x) - n\xi_m(x)\psi'_m(nx)} \quad (2)$$

Here $x = k_0 r_0$, k_0 is the free-space wavenumber, $\psi_m(x)$ and $\xi_m(x)$ are the Riccati–Bessel functions, and the primes indicate derivatives with respect to the arguments. The scattering coefficients a_1 and b_1 are related to the electric and magnetic dipolar responses of the sphere, respectively. And the coherence effect, referring to the coupling interaction between the electric and magnetic dipole resonances, mainly depends on the geometrical dimensions and permittivity of the particles (Figure 1). The weakened coherence effect implies that the electric and magnetic resonances happen at frequencies far from each other. Such coherence is governed by the proximity of the lowest-frequency dispersion peaks of a_1 and b_1, and can be enhanced by decreasing the dielectric constant, e.g., from 120 to 16.5 and increasing the radius of the particle, e.g., from 1.0 to 9.0 mm as illustrated in Figure 1. Analytical solutions for the scattering coefficients of the coherent and noncoherent cases are plotted in Figure 1a,b, respectively. The insets in these respective diagrams demonstrate the EM field distribution within the particle for these two distinct cases. The noncoherent case exhibits a localized resonance of the EM field whereas the coherent case is less confined as seen in the insets of Figure 1. The pure magnetic dipole response is denoted by points B and E in Figure 1, while points D and F show the pure electric dipole response. For the coherent case, points A and C exhibit a special circumstance where the scattering coefficients are $a_1 = b_1$ and $a_1 = b_1^*$. At these points, the hybrid electric and magnetic dipole responses at the same frequency (insets A and C) provide both electric and magnetic responses baring a strong resemblance to the metamaterial-based fishnet structure. Such coherence effects have resulted in several exotic scattering phenomena,[27–29] including zero-backward scattering at $a_1 = b_1$, and nearly zero-forward scattering at $a_1 = b_1^*$. In these cases, however, the wavelength is on the same order of the particle size. The increase of the permittivity and the decrease of the size of the particles weaken the coherence effect, i.e., the frequency separation between the electric and magnetic resonances enlarges, and purer magnetic resonance can be observed. Therefore, as shown in Figure 1b, the diameter of particle is much smaller than the first resonance wavelength of b_1 ($\lambda/2r_0 \approx 10$), making the long wavelength approximation satisfied. The EM responses of the dielectric cubes with different dimensions but with the fixed dielectric constant (Figure S1, Supporting Information) further confirm that the permittivity of particle plays a significant role in the coherence effect.

Mie resonance appears for any geometry, but only Mie scattering for regular geometries (such as spheres and cylinders) can be analytically calculated. For other geometries like cubes, numerical method rather than analytical calculation is used to identify the magnetic dipole responsible for the resonance. To simplify the fabrication process, dielectric $CaTiO_3$ cubes (permittivity $\varepsilon = 120+0.1i$ and sidelength $l = 2.00$ mm) rather than spheres were used as subwavelength-resonant particles to interact with the EM wave. These interactions are characterized by measuring the electric field distribution using a 2D electric field mapping system[17] (**Figure 2**a) that provides detailed wave transmission and direct phase control information compared to the directional radiation measurement commonly employed in recent studies.[35] The cross sections of E and H field within the dielectric cube indicate the nature of responses at A and B points are magnetic and electric resonances, respectively (Figure 2b). Interactions between cylindrical waves generated by a monopole and the single or several dielectric particles are studied near their first Mie resonance and shown in Figure 2. For the single-particle case (Figure 2c), the cylindrical wavefront is broken at the magnetic resonance (approximately 11.55 GHz in experiment and 11.60 GHz in simulation) and becomes an ellipse with the prolate and short axes along the x- and y-axes, respectively. The wave mainly propagates outward along the short axis, akin to the zero-backward scattering case. However, the cylindrical wavefront will not be influenced for frequencies far from resonance (Figure S2, Supporting Information). In order to study how the field map is affected by a nonsymmetric particle arrangement along the x-and y-axes, particles were placed laterally from the propagation direction (along the x-axis). Figure 2 shows that as the number of particles increases, the wavefront gradually changes to an ellipse with a much higher aspect ratio, providing a longer linear wavefront and better directional emission. At the same time, the working frequency has a small redshift compared to that of a single particle. This is because each particle can be seen as a magnetic dipole with the moment along the x-direction; increasing the number of particles along the x-direction enhances the attractive interaction and results in a decrease of the restoring force of the magnetic resonator and thus the decrease of the resonance

Adv. Mater. 2015,
DOI: 10.1002/adma.201502298

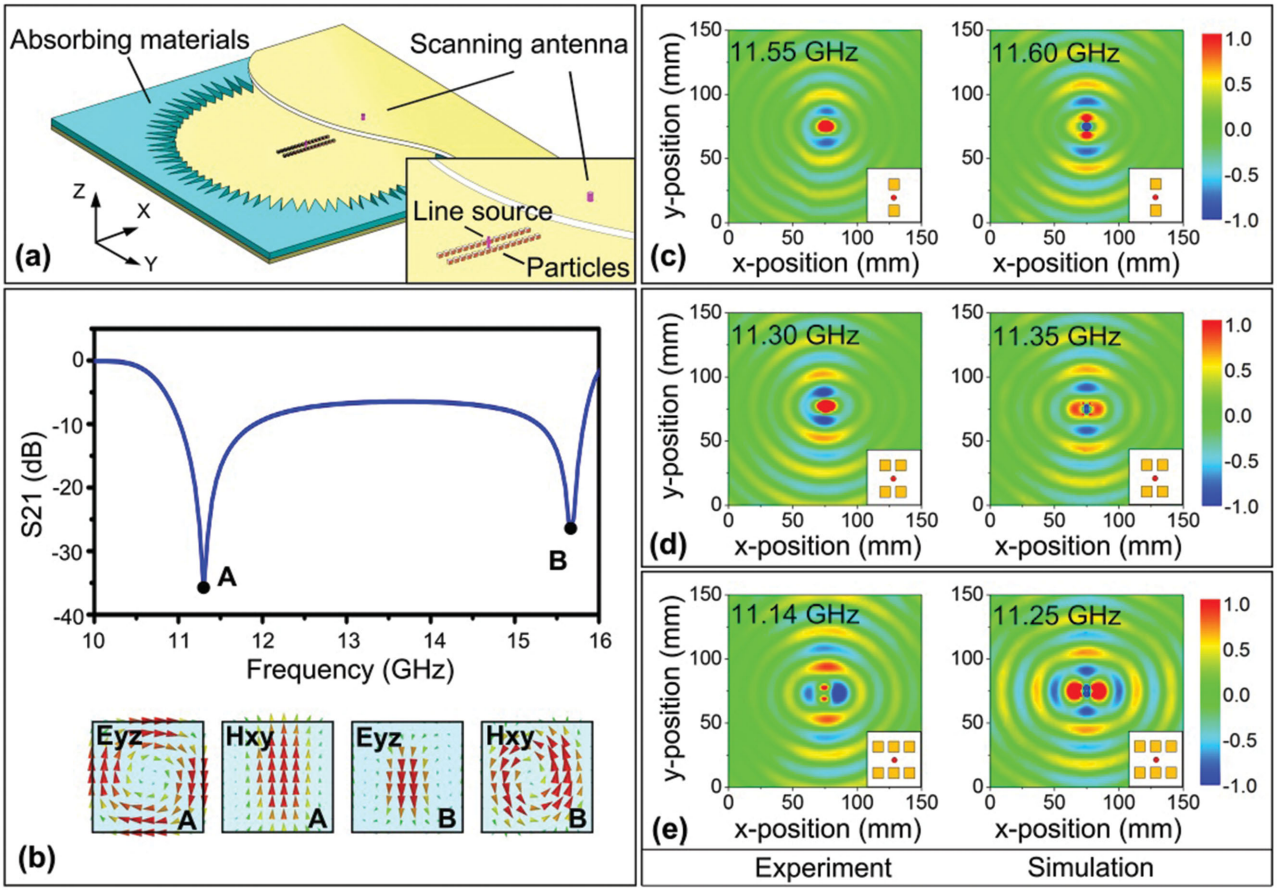

Figure 2. Interaction between single/several dielectric particles and EM wave. a) Schematic of the electric field measurement system; b) The S-parameters and corresponding electromagnetic field distribution within the particle; c) one-pair particles; d) two-pair particles; e) three-pair particles. Left and right figures correspond to the experiments and simulations. The separation between the cubes is 2.70 mm in the *x*-direction, and the separation between the monopolesource and particle lines is 2.70 mm in the *y*-direction.

frequency. According to Figure 2, the experiments show good consistency with the simulations. It shows that with the weak coherence, these subwavelength particles can also control the wave propagation near the first Mie resonance. The particle arrays exhibit the dipole radiation effect, where the array is excited by a monopole source and then reradiates as a magnetic dipole, seen from the fact that this wavefront modulation occurs at the magnetic resonance.

Having demonstrated efficient wave modulation with a single dielectric particle, the next step is to consider how linear particle arrays may impact the performance and provide novel EM mechanisms. The experimental and simulated electric field maps of the different layers of particle arrays (Figure S3c, Supporting Information) are shown in **Figure 3**. The EM field at a nonworking frequency of 8.00 GHz (Figure 3a) shows a typical concentric circular wavefront distribution like the cylindrical wave excited by a monopole source, that is to say, the sample has no influence on the EM wave at all. While at the working frequency of 12.03 GHz, the circular wavefront of the emitted cylindrical wave is broken and translates into a plane wave, indicating how a single layer of dielectric subwavelength particles provides efficient control to modify the directionality of the emission (Figure 3b). For each particle in the linear array, the distances between the monopole source and the particles are different, so the phase along the linear array should not be the same for a conventional medium. However at the working frequency, we see that nearly the same phase occurs along the entire linear array, except for some minor differences near the monopole and a phase delay outside the samples. This equiphase effect is exactly a typical characteristics of the zero-index effect.

For a single-layered particle array, the effective parameters were retrieved using the method described in ref.[38] and shown in **Figure 4**a. It shows that the permeability becomes negative or zero at frequencies above the first Mie resonance and thus the refractive index is also zero for even only one layer of particle array. The clearly visible antiresonance and negative imaginary part of permittivity near the first Mie magnetic resonance are artifacts and arise from the periodicity of the unit cells, which could be reduced or eliminated by moving the magnetic resonance to sufficiently low frequency.[39] It may not seem reasonable to treat a single layer of subwavelength particle array as an effective medium due to the ratio of the sample's size compared to the wavelength. In order to demonstrate the validity of the effective medium assumption, we further retrieved the effective parameters

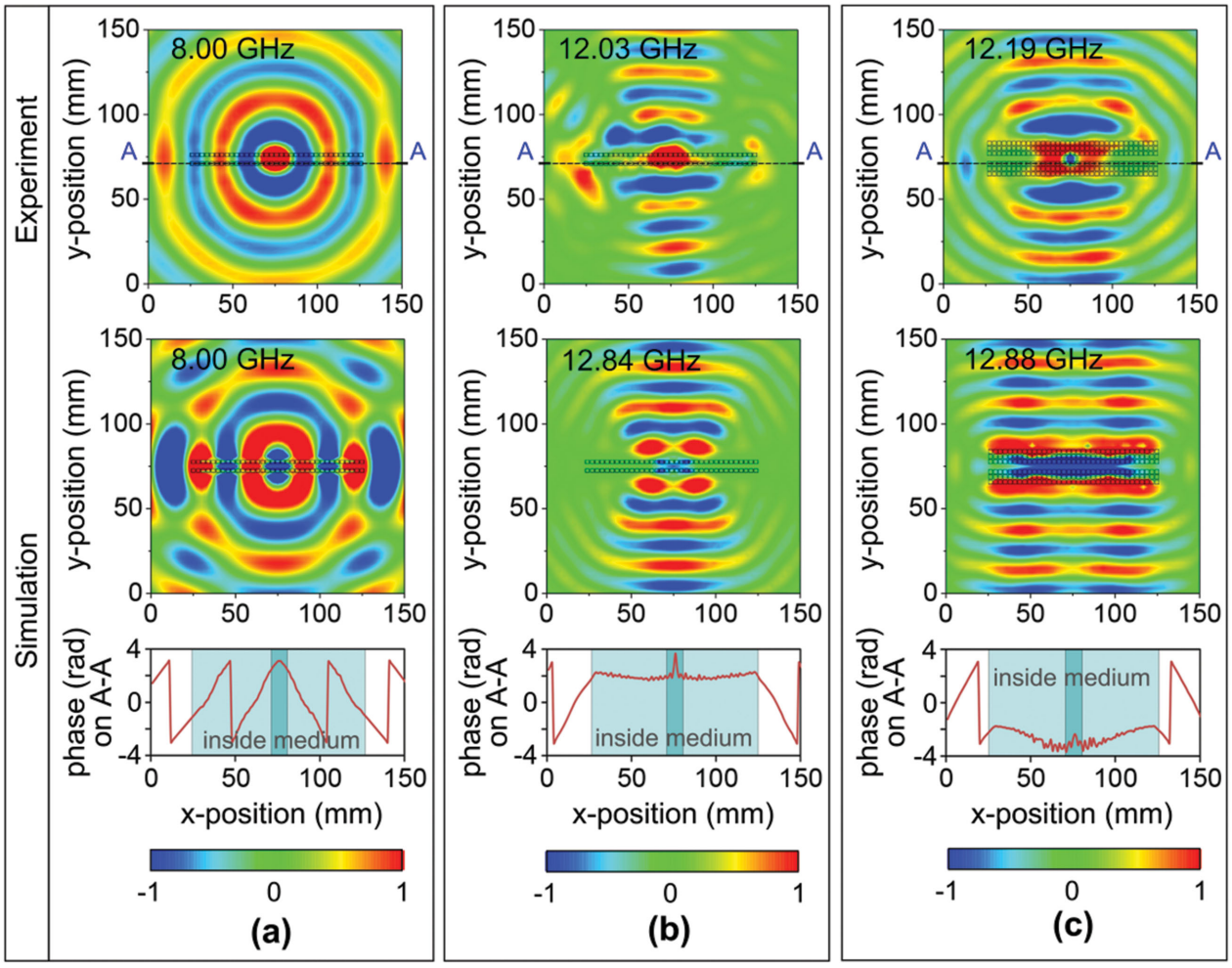

Figure 3. Electric field mapping of different layers of linear array samples. a) A single layer at nonworking frequency; b) a single layer at working frequency; c) three layers at working frequency. Top, middle, and bottom figures correspond to the experiment, simulation, and the phase distributions at the cross section of the particle array.

for 2 and 3-layer particle arrays (see Figure 4b). The results show that the effective index can be zero and maintain consistency while increasing the number of layers. It should be noted that though the dispersion of the effective permittivity becomes abnormal at the magnetic resonance, that of the magnetic resonance remains causal. In our case, the working frequency in concern is off and higher than the magnetic resonance.

We also substituted the particles by an equivalent medium with these extracted effective parameters ($\varepsilon = 4.315 + 0.003i$, $\mu = -0.003 + 0.007i$, $n = 0.103 + 0.153i$) from Figure 4 at 12.48 GHz and calculated the field distribution (Figure S4, Supporting Information). Compared with the simulation and experiment results in Figure 3, this equivalent medium shows a highly similar field distribution. Therefore, in principle, a single layer of particle array, with thickness $d \approx \lambda/10$, can be seen as an effective medium with zero refractive index, since the particle array is still not atomically thin and it is reasonable to apply the effective parameters in order to describe such subwavelength layers. In addition, the experiments agree well with the simulations (Figure 3). The slight deviation of the wavefront from an absolutely parallel wavefront in the experiments may be considered due to the nonuniformity in the size and dielectric constant of the cubes and the lattice constant. We note that the distance between particles, i.e. the filling ratio, can modify the value of the effective permeability but has less influence on the response frequency (Figure S5, Supporting Information).

Since the unit cell of the array has a regular cube structure, the fabricated zero-index medium is isotropic in all three dimensions. This medium demonstrates an invariant phase throughout, which cannot be realized in hyperbolic anisotropic zero-index materials. According to Snell's Law, the emergent wave will be perpendicular to the surface after propagating through the isotropic zero-index medium. With an increase in the number of layers along the propagation direction (Figure 3c), the control of wave directionality and the zero-index-effect are still observed, though not significantly

Adv. Mater. **2015**,
DOI: 10.1002/adma.201502298

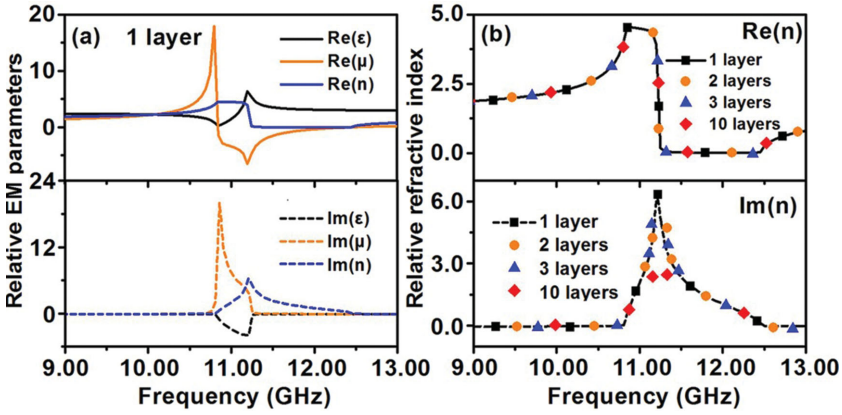

Figure 4. Retrieved electromagnetic parameters for different layers, which indicates that even only one layer particle (subwavelength thickness) can be described successfully by effective medium theory. a) Permitivity, permeablity, and refractive index for one layer cube; b) refraction index for different layer cubes.

enhanced. At the same time, we find that the transmittance decreases with the increase in the number of layers along the propagation direction. This effect can be understood through the following transmission calculation in the near-zero-index medium. The inherent loss of the cube material is also studied, but found not dominant here.

For a TE polarized wave, the transmission coefficient t of one layer of homogenous medium 2 is

$$t = 1 - \frac{r_{12} + r_{23}e^{2i\beta}}{1 + r_{12}r_{23}e^{2i\beta}} \tag{3}$$

where $\beta = (2\pi / \lambda_0)\sqrt{\varepsilon_2\mu_2}\,d\cos\theta_2$, ε_2 and μ_2 are the relative permittivity and permeability of the second medium, d is the thickness of the second medium, θ_j (j = 1, 2, 3) is the angle between the light and the normal of the interface, and λ_0 is the vacuum wavelength. When media 1 and 3 are vacuum

$$r_{12} = \frac{\cos\theta_1 - \sqrt{\frac{\varepsilon_2}{\mu_2}}\cos\theta_2}{\cos\theta_1 + \sqrt{\frac{\varepsilon_2}{\mu_2}}\cos\theta_2} \tag{4}$$

$$r_{23} = \frac{\sqrt{\frac{\varepsilon_2}{\mu_2}}\cos\theta_2 - \cos\theta_1}{\sqrt{\frac{\varepsilon_2}{\mu_2}}\cos\theta_2 + \cos\theta_1} \tag{5}$$

Substituting Equations (4) and (5) into Equation (3), the transmittances T where $\varepsilon_2 \to 0$ and $\mu_2 \to 0$ are

$$\lim_{\varepsilon_2\to 0} T = \lim_{\varepsilon_2\to 0} |t|^2 = \frac{1}{\pi^2 d^2 \mu_2^2 \cos^2\theta_1 / \lambda_0^2 + 1} \tag{6}$$

$$\lim_{\mu_2\to 0} T = \lim_{\mu_2\to 0} |t|^2 = \frac{\cos^2\theta_1}{\pi^2 d^2 \varepsilon_2^2 \cos^4\theta_2 / \lambda_0^2 + \cos^2\theta_1} \tag{7}$$

Considering a case of normal incidence, $\theta_1 = \theta_2 = 0$, Equations (6) and (7) become

$$\lim_{\substack{\varepsilon_2\to 0 \\ \mu_2 = 1}} T = \lim_{\substack{\mu_2\to 0 \\ \varepsilon_2 = 1}} T = \frac{1}{\pi^2 d^2 / \lambda_0^2 + 1} \tag{8}$$

According to Equation (8), the permittivity ε and permeability μ are highly symmetric. When either of these parameters approaches zero, the transmittance T decreases monotonically while the thickness of the near-zero-index medium increases. This explains why the transmittance of a single-layer particle array is larger than that of a three-layer array. This further verifies that the EM wave controlling mechanism based on the Mie resonance has more potential applications for miniaturizing devices.

As previously shown, the subwavelength particle array exhibits a near-zero-index near the first Mie resonance and is capable of modulating a wave with the outgoing wavefront perpendicular to the interface. This directional modulation depends entirely on the shape of the medium interface. This

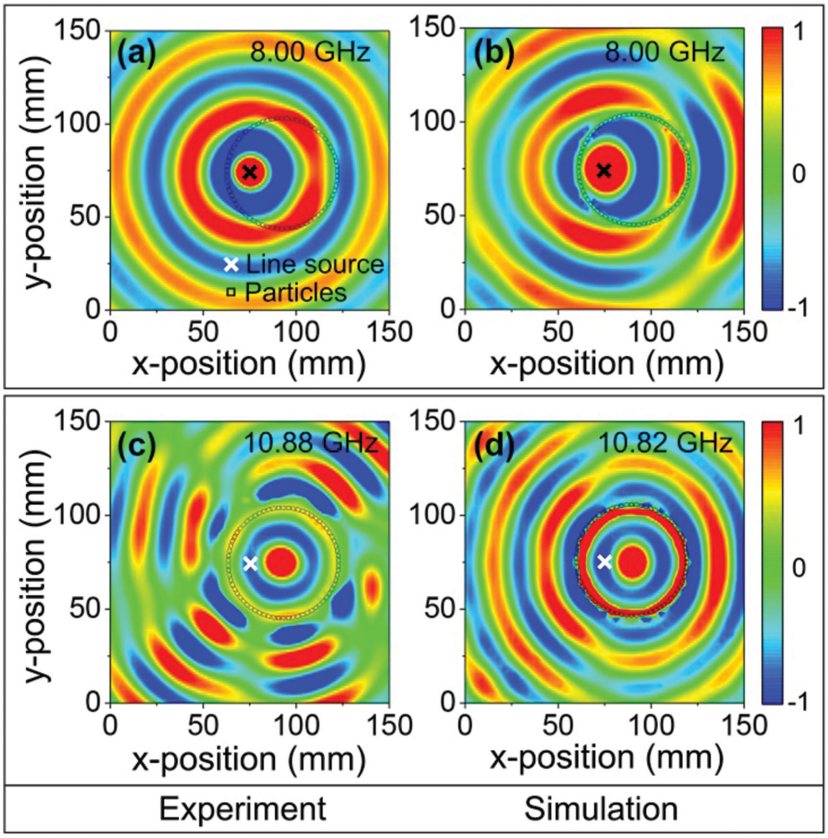

Figure 5. Electric field mapping of the circular array samples. a) Experiments and b) simulations at the nonworking frequency; c) experiments and d) simulations at the working frquency. Where "×" indicates the position of the monopole source.

property provides extra flexibility to precisely control the wavefront to take on arbitrary shapes by changing the interface of the proposed EM device. The circular sample (Figure S3d, Supporting Information) is fabricated by assembling the particles into a circular array, and a monopole source is eccentrically placed inside the sample. At the nonworking frequency, the circular sample has no influence on the emission of the monopole and exhibits a concentric wavefront centered at the monopole (**Figure 5**a). However, at the working frequency of 10.88 GHz, the equiphase surface of the wave becomes a series of concentric circles centered at the sample's center instead of the monopole source (named as the "eccentric effect") near the first Mie resonance (Figure 5b).

The nonzero reflectance leads to the interference inside the circle and thus the amplitude of the wave inside the sample forms a concentric circular wavefront with the circular array. The reflection and interference effects in experiment are more obvious than those observed in simulations, which may arise from the fabrication errors of the samples, such as the nonuniformity of geometry dimensions and dielectric constant of the cubes. And the round shaped array of cubes has stronger influence on the wavefront than that of the rectangular shaped ones, which makes the effect of nonuniformity more obvious. The particle array sample can be used as a spatial power combiner for omnidirectional radiation to obtain high-efficiency spatial power and improve the directionality of wave emission. At the same time, it can be applied to optical camouflage, i.e., the virtual source (the geometric center of the circle sample) is produced while the real source is concealed.

In addition, active control of EM wave propagation has a wide range of applications. It is relatively complicated to tune the constituting structures of metamaterials because the geometrical dimension or surrounding medium has to be varied. Fortunately, the dielectric subwavelength particles have an intrinsic temperature-dependent permittivity and thus the first Mie resonance of the dielectric sphere is a function of radius and permittivity of the sphere, $\omega \approx \pi c / (r_0 \sqrt{\varepsilon})$.[36] Therefore, a variation in the spectral location of the Mie resonance can be easily realized by changing the sample temperature and thus the wavefront can be adjusted. The electric field distributions in a linear array of particles are measured and shown in **Figure 6**. The transmission dip corresponding to the first Mie resonance experiences a blueshift (12 MHz $°C^{-1}$) and the wavefront translates from planar (Figure 6b) to irregular (Figure 6d) with the temperature variation from 15 to 25 °C at a frequency of 12.03 GHz. The wavefront becomes planar (Figure 6e) again at a temperature of 25 °C and a frequency of 12.12 GHz. This result provides the possibility to adjust the working band of the zero-index device and realize multiband tunable control in the future.

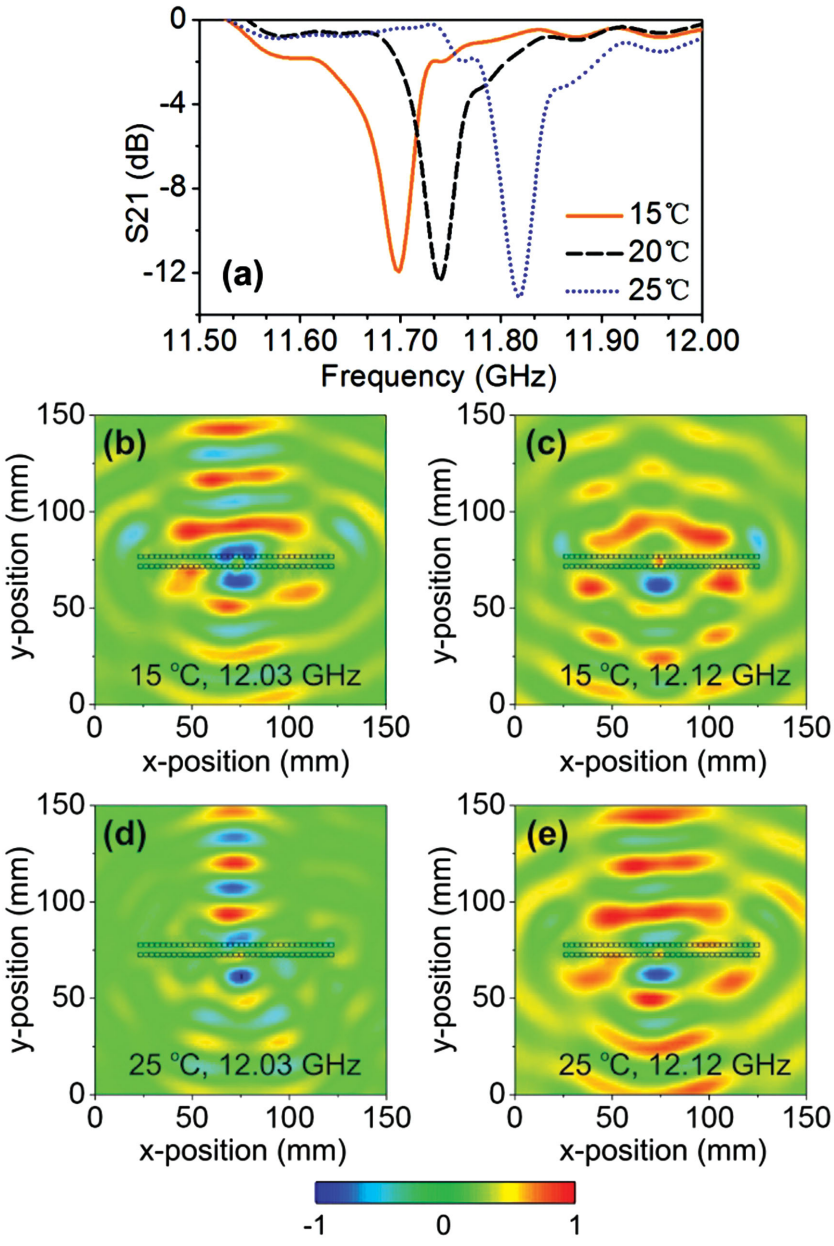

Figure 6. Temperature controllable near-zero-index effect in a linear array of particles. a) Transimission spectra of a dielectric cube with different temperatures; electric field distribution of 12.03 GHz at temperatures of b) 15 °C, d) 25 °C; electric field distribution of 12.12 GHz at temperatures of c) 15 °C, e) 25 °C.

The localized resonance in the high index dielectric subwavelength particles, arising from the magnetic Mie resonance, is responsible for phase and wavefront control of the particle layers. A decrease in the particle size and an increase in the permittivity make the effective medium theory appropriate for application in the theoretical analysis of the subwavelength particle arrays. Differing from the zero-backward and almost

Adv. Mater. **2015**,
DOI: 10.1002/adma.201502298

zero-forward scattering phenomena, which are related to the interference coupled between electric and magnetic dipolar responses, we find another novel isotropic equiphase control behavior. This equiphase control can be seen in even one layer of a particle array interacting with a cylindrical wave and originates from the MNZ excited by a single magnetic response. The underlying physics is different from the zero-index attained in photonic crystals or hyperbolic materials. For photonic crystals, Bragg diffraction and Dirac cone are responsible for the zero index. Although the all-dielectric photonic crystal is used instead of metallic structures, the response is still anisotropic only for the TM mode. Furthermore, the lattice constant of photonic crystal is about the same scale as the optical wavelength, not subwavelength. And photonic crystal consists of many periodic-arrayed unit cells along the wave propagation direction, that is, only one layer cannot realize this special effect. But for our case, only one layer of particle array can exhibit isotropic μ-near-zero effect and control ten-times-longer wavelength light. For hyperbolic materials, it is anisotropic zero-index-like effect. It can control the wave trasmission direction, but the wave phase inside the medium cannot be kept the same. Our material may even resemble metasurfaces, which also exhibit wavefront control with one layer of unit cells. But there are some distinct differences. In our case, the layer of particles essentially operates as an isotropic effective medium sheet and the observed equiphase effect is due to the near-zero index. The study of equiphase in the cross section of the particle array further provides a method to judge whether a medium can be seen as an effective medium. Particle arrays with higher permittivity can also control the wavefront (Figure S6, Supporting Information). Similar functionality can be extended to THz and optical frequency ranges where higher index particles are also available.[40–42] In summary, we show a single layer of subwavelength dielectric particles that merges and utilizes the localized Mie resonance, effective medium theory, and wavefront control science and technology, which opens new avenues in manipulating waves and developing more compact optical devices from the microwave to THz regime in unprecedented ways.

Experimental Section

Device and Sample Fabrication: Samples were prepared by assemblying dielectric cubes in specially designed templates. Here the $CaTiO_3$ cubes were fabricated by an inner circle slicer and a dicing cutter widely used in IC manufacturing. The templates were fabricated using a laser cutter. To decrease the surrounding permittivity of the dielectric cubes, the teflon templates with 0.5 mm thickness were chosen to construct the hollow 3D samples (Figure S3, Supporting Information).

Measurements: The 2D electric field mapping system (Figure S7, Supporting Information) was designed and used to measure the electric field as it propagated in and around the samples. Combined with a vector network analyzer (Agilent E5071C), the electric field distribution in an area of 400 mm × 400 mm could be automatically measured point-by-point.

Supporting Information

Supporting Information is available from the Wiley Online Library or from the author.

Acknowledgments

This work was supported by the National High Technology Research and Development Program of China (Grant No. 2012AA030403), the National Natural Science Foundation of China (Grant Nos. 61275176, 61101044, 11372248, 91123033, and 51323006), the Program for New Century Excellent Talents in University (NCET-13-0337), and the Chinese State Key Laboratory of Tribology. Work at Ames Lab (theory) was partially supported by the U.S. Department of Energy, Office of Basic Energy Science, Division of Materials Sciences and Engineering under contract No. DE-AC02-07CH11358, the U.S. Office of Naval Research (Simulations) award No. N00014-14-1-0474, and the European Research Council under the ERC Advanced Grant No. 320081 at FORTH. The authors gratefully acknowledge discussions with Dr. L. Kang, J. B. Sun, A. Jain, and Prof. C. W. Qiu.

Received: May 13, 2015
Revised: July 5, 2015
Published online:

[1] J. B. Pendry, *Nat. Mater.* **2006**, *5*, 763.
[2] D. K. Gramotnev, S. I. Bozhevolnyi, *Nat. Photonics* **2010**, *4*, 83.
[3] S. A. Maier, P. G. Kik, H. A. Atwater, S. Meltzer, E. Harel, B. E. Koel, A. A. G. Requicha, *Nat. Mater.* **2003**, *2*, 229.
[4] R. H. Fan, Y. Zhou, X. P. Ren, R. W. Peng, S. C. Jiang, D. H. Xu, X. Xiong, X. R. Huang, M. Wang, *Adv. Mater.* **2015**, *27*, 1201.
[5] R. A. Shelby, D. R. Smith, S. Schultz, *Science* **2001**, *292*, 77.
[6] S. Zhang, W. Fan, N. C. Panolu, K. J. Malloy, R. M. Osgood, S. R. J. Brueck, *Phys. Rev. Lett.* **2005**, *95*, 137404.
[7] G. Dolling, M. Wegener, C. M. Soukoulis, S. Linden, *Opt. Lett.* **2007**, *32*, 53.
[8] J. Zhou, E. N. Economou, Th. Koschny, C. M. Soukoulis, *Opt. Lett.* **2006**, *31*, 3620.
[9] J. Valentine, S. Zhang, T. Zentgraf, E. Ulin-Avila, D. A. Genov, G. Bartal, X. Zhang, *Nature* **2008**, *455*, 376.
[10] S. Enoch, G. Tayeb, P. Sabouroux, N. Guerin, P. A. Vincent, *Phys. Rev. Lett.* **2002**, *89*, 213902.
[11] R. W. Ziolkowski, *Phys. Rev. E* **2004**, *70*, 046608.
[12] N. Engheta, *Science* **2013**, *340*, 286.
[13] J. B. Pendry, *Phys. Rev. Lett.* **2000**, *85*, 3966.
[14] N. Fang, H. Lee, C. Sun, X. Zhang, *Science* **2005**, *308*, 534.
[15] J. Sun, M. I. Shalaev, N. M. Litchinitser, *Nat. Commun.* **2015**, *6*, 7201.
[16] J. B. Pendry, D. Schurig, D. R. Smith, *Science.* **2006**, *312*, 1780.
[17] D. Schurig, J. J. Mock, B. J. Justice, S. A. Cummer, J. B. Pendry, A. F. Starr, D. R. Smith, *Science* **2006**, *314*, 977.
[18] A. Mirzaei, A. E. Miroshnichenko, I. V. Shadrivov, Y. S. Kivshar, *Sci. Rep.* **2015**, *5*, 9574.
[19] J. Sun, E. Timurdogan, A. Yaacobi, E. S. Hosseini, M. R. Watts, *Nature* **2013**, *493*, 195.
[20] J. A. Schuller, R. Zia, T. Taubner, M. L. Brongersma, *Phys. Rev. Lett.* **2007**, *99*, 107401.
[21] L. Peng, L. Ran, H. Chen, H. Zhang, J. A. Kong, T. M. Grzegorczyk, *Phys. Rev. Lett.* **2007**, *98*, 157403.
[22] B. I. Popa, S. A. Cummer, *Phys. Rev. Lett.* **2008**, *100*, 207401.
[23] Q. Zhao, L. Kang, B. Du, H. Zhao, Q. Xie, X. Huang, B. Li, J. Zhou, L. Li, *Phys. Rev. Lett.* **2008**, *101*, 027402.
[24] F. Zhang, Q. Zhao, L. Kang, J. Zhou, D. Lippens, *Phys. Rev. B* **2009**, *80*, 195119.
[25] A. B. Evlyukhin, S. M. Novikov, U. Zywietz, R. L. Eriksen, C. Reinhardt, S. I. Bozhevolnyi, B. N. Chichkov, *Nano Lett.* **2012**, *12*, 3749.
[26] A. I. Kuznetsov, A. E. Miroshnichenko, Y. H. Fu, J. B. Zhang, B. Luk'yanchuk, *Sci. Rep.* **2012**, *2*, 492.

[27] S. Person, M. Jain, Z. Lapin, J. J. Sáenz, G. Wicks, L. Novotny, *Nano Lett.* **2013**, *13*, 1806.
[28] J. M. Geffrin, B. García-Cámara, R. Gómez-Medina, P. Albella, L. S. Froufe-Pérez, C. Eyraud, F. Moreno, *Nat. Commun.* **2012**, *3*, 1171.
[29] Y. H. Fu, A. I. Kuznetsov, A. E. Miroshnichenko, Y. F. Yu, B. Luk'yanchuk, *Nat. Commun.* **2013**, *4*, 1527.
[30] W. Liu, A. E. Miroshnichenko, D. N. Neshev, Y. S. Kivshar, *ACS Nano* **2012**, *6*, 5489.
[31] P. Moitra, Y. Yang, Z. Anderson, I. I. Kravchenko, D. P. Briggs, J. Valentine, *Nat. Photonics* **2013**, *7*, 791.
[32] R. Liu, Q. Cheng, T. Hand, J. J. Mock, T. J. Cui, S. A. Cummer, D. R. Smith, *Phys. Rev. Lett.* **2008**, *100*, 023903.
[33] B. Edwards, A. Alu, M. E. Young, M. Silveirinha, N. Engheta, *Phys. Rev. Lett.* **2008**, *100*, 033903.
[34] X. Huang, Y. Lai, Z. H. Hang, H. Zheng, C. T. Chan, *Nat. Mater.* **2011**, *10*, 582.
[35] Q. Cheng, W. X. Jiang, T. J. Cui, *Phys. Rev. Lett.* **2012**, *108*, 213903.
[36] Q. Zhao, B. Du, L. Kang, H. Zhao, Q. Xie, B. Li, X. Zhang, J. Zhou, L. Li, Y. G. Meng, *Appl. Phys. Lett.* **2008**, *92*, 051106.
[37] C. F. Bohren, D. R. Huffman, *Absorption and Scattering of Light by Small Particles*, John Wiley and Sons, New York **1983**.
[38] D. R. Smith, S. Schultz, P. Markoš, C. M. Soukoulis, *Phys. Rev. B* **2002**, *65*, 195104.
[39] Th. Koschny, P. Markoš, E. N. Economou, D. R. Smith, D. C. Vier, C. M. Soukoulis, *Phys. Rev. B* **2005**, *71*, 245105.
[40] C. Rockstuhl, F. Lederer, C. Etrich, T. Pertsch, T. Scharf, *Phys. Rev. Lett.* **2007**, *99*, 017401.
[41] A. B. Evlyukhin, C. Reinhardt, A. Seidel, B. S. Luk'yanchuk, B. N. Chichkov, *Phys. Rev. B* **2010**, *82*, 045404.
[42] S. N. Sheikholeslami, H. Alaeian, A. L. Koh, J. A. Dionne, *Nano Lett.* **2013**, *13*, 4137.

Adv. Mater. **2015**,
DOI: 10.1002/adma.201502298